Supporting Information

Pyridal[2,1,3]thiadiazole as Strong Electron-Withdrawing and Less Steric Hindrance Acceptor For Highly Efficient Donor-Acceptor type NIR Materials

Jianxia Jiang, Xianglong Li, Muddasir Hanif, Jiadong Zhou, Dehua Hu,* Shijian Su, Zengqi Xie, Yu Gao, Bing Yang, Yuguang Ma*

Table of Contents

Section 1. Materials and Method

General Methods: All solvents and reagents used for synthesis were purchased from Aldrich or Acros and used as received without further purification.

^{1}H and ^{13}C NMR data were collected with a Bruker AVANCE Digital 600 MHz NMR workstation. All data were using tetramethylsilane (TMS) as the internal standard. Matrix-Assisted Laser Desorption Ionization time-of-flight (MALDI-TOF) mass spectra were performed on a Bruker Autoflex III Smartbeam. For differential scanning calorimetry (DSC), a Netzsch DSC 209 apparatus with a heating and cooling rate of 10 °C min^{-1} under N_2 flow was used. Thermogravimetric analyses (TGA) were performed on a Netzsch TG 209 apparatus under a N_2 flow at a heating rate of 10 °C min^{-1}. Cyclic voltammetry (CV) was performed on a CHI760D electrochemical workstation. The measurements were used Glassy Carbon working electrode and Pt wire counter electrode at a scanning rate of 50 mV s^{-1} against a Ag/Ag$^+$ (0.01 M of AgNO$_3$ in acetonitrile) reference electrode in a nitrogen-saturated anhydrous acetonitrile and dichloromethane (DCM) solution of 0.1 mol L^{-1} Bu$_4$NPF$_6$ as the electrolyte. The measurement was calibrated against ferrocene/ferrocenium redox system. Absorption spectra were recorded on a UV-3600 spectrophotometer from Shimadzu. Photoluminescence (PL) spectra were received on a Jobin-Yvon spectrofluorometer.

Device Fabrication and Characterization: The ITO-coated glass substrates used as anode were cleaned with acetone, deionized water and isopropanol in an ultrasonic bath, and then dried in an oven at 90 °C. The devices were fabricated by vacuum evaporation of the organic and metal materials onto the ITO coated glass substrates at 5 × 10^{-4} Pa. Before the fabrication of the devices, the compounds were further purified by sublimation. The devices were constructed by evaporation organic layers with a deposition rate of the 1.0-2.0 Å s^{-1}. The deposition rate of LiF and Al were 0.1 Å s^{-1} and 4.0 Å s^{-1}, respectively. The thickness of the deposited material was monitored by an oscillating quartz thickness monitor. Electroluminescence (EL) spectra and CIE coordinates were measured using a PR705 spectra

scan spectrometer. The luminance and current density versus driving-voltage characteristics were measured by combining the spectrometer CS200 with a Keithley model 2420 programmable voltage-current source meter. All measurements were carried out under ambient conditions and at room temperature.
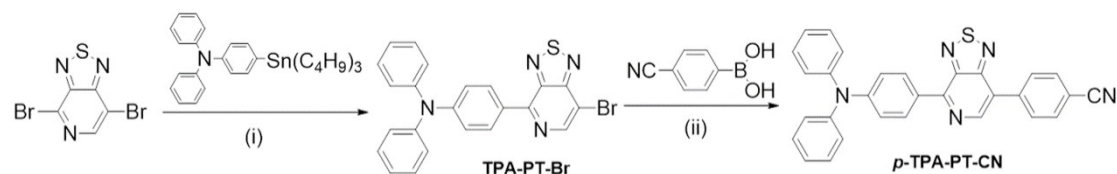
(i) Pd(PPh$_3$)$_4$,THF, 80°C, 36h.
(ii) Pd(PPh$_3$)$_4$, 2M K$_2$CO$_3$, Methanol, Toluene(1:1:2), 90°C, 24h.

Scheme S1. Chemical structures and synthetic route of *p*-TPA-PT-CN.

Synthesis of TPA-PT-Br

4,7-dibromo-[1,2,5]thiadiazolo[3,4-c]pyridine(0.50 g, 1.71 mmol), N,N-diphenyl-4-(tributylstannyl)aniline (0.90 g, 1.69 mmol), Pd(PPh$_3$)$_4$ (0.20 g, 10 mol%), 20 ml THF were first mixed. The reaction mixture was stirred at 90° C for 36h under a nitrogen atmosphere. After cooling to room temperature, the mixture was washed by water and extracted with chloroform consecutively. The organic phase was collected and further dried with anhydrous MgSO$_4$. After evaporation of the solvent, the residue was purified by column chromatography on silica gel using a petroleum ether/dichloromethane mixture (3:1), and the pure product of compound TPA-PT-Br was finally obtained (0.31 g, yield 40 %). ^{1}H NMR (CDCl$_3$, 600 MHz, δ): 8.67 (s, 1H, Py-H), 8.42-8.40 (d, 2H, J = 8.41 Hz, Ar-H), 7.26-7.23 (t, 4H, J = 7.25 Hz, Ar-H), 7.14-7.09 (m, 6H, Ar-H), 7.06-7.04 (t, 4H, J = 7.05 Hz, Ar-H). MALDI-TOF-MS (m/z): C$_{23}$ H$_{15}$N$_4$SBr, 459.10.

Synthesis of *p*-TPA-PT-CN

TPA-PT-Br (0.55 g, 1.20 mmol), 4-Cyanophenylboronic acid (0.25 g, 1.80 mmol), Pd(PPh$_3$)$_4$ (0.14g, 10 mol%), K$_2$CO$_3$ (1.38 g, 2 mmol), distilled water (5 mL), methanol (5 ml), and toluene (10 mL) were first mixed. The mixture was cooled and deoxidize under a nitrogen atmosphere for 3 times. Then the reaction mixture was stirred at 90°C for 36 h under a nitrogen

atmosphere. After cooling to room temperature, the mixture was washed by water and extracted with chloroform consecutively. The organic phase was collected and further dried with anhydrous $MgSO_4$. After evaporation of the solvent, the residue was purified by column chromatography on silica gel using a petroleum ether/dichloromethane mixture (2:1), and the pure product of compound *p*-TPA-PT-CN was finally obtained. (0.53 g, 1.09 mmol, yield 91%).

^{1}H NMR (CDCl$_3$, 600 MHz, δ): 8.72 (s, 1H, Py-H), 8.51-8.49 (d, 2H, J = 8.50 Hz, Ar-H), 8.09-8.08 (d, 2H, J = 8.08 Hz, Ar-H), 7.78-7.76 (d, 2H, J = 7.77 Hz, Ar-H), 7.27-7.24 (t, 4H, J = 7.25 Hz, Ar-H), 7.15-7.11 (m, 6H, J = 7.13 Hz, Ar-H), 7.07-7.04 (t, 2H, J = 7.05 Hz, Ar-H). ^{13}C NMR (CDCl$_3$, 600 MHz, δ): 155.38, 152.07, 149.50, 148.60, 145.80, 142.47, 138.35, 131.53, 130.15, 128.50, 124.66, 123.20, 122.75, 120.19, 117.71, 112.80, 110.99. MALDI-TOF-MS (m/z): $C_{30}H_{19}N_5S$, 481.0611. Elemental analysis calculated [%] for $C_{30}H_{19}N_5S$: C, 74.82; H, 3.98; N, 14.54; S, 6.66, found: C, 74.53; H, 3.93; N, 14.63; S, 6.63
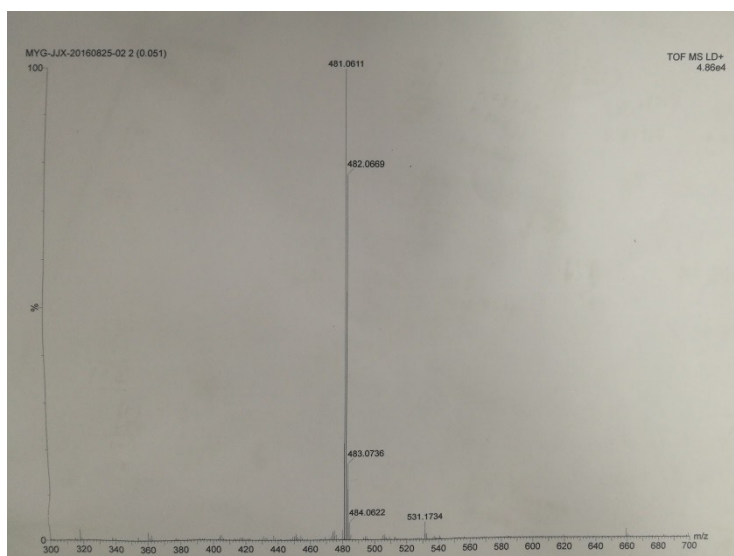
Figure S1 The MALDI-TOF-MS (m/z) graph of *p*-TPA-PT-CN.

4444444444444
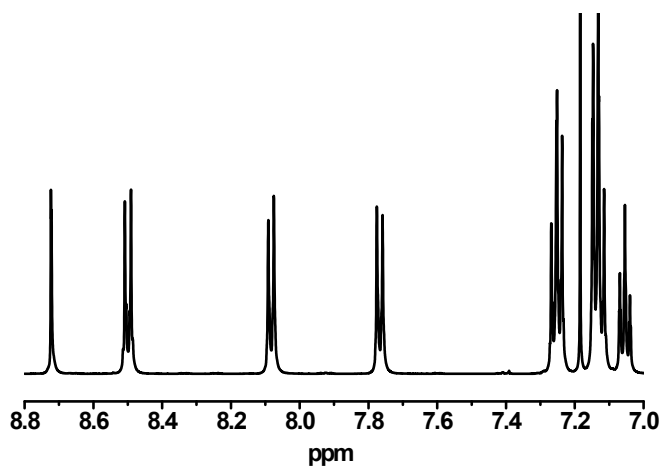
Figure S2 The ^{1}H NMR (CDCl$_3$, 600 MHz) graph of p-TPA-PT-CN.
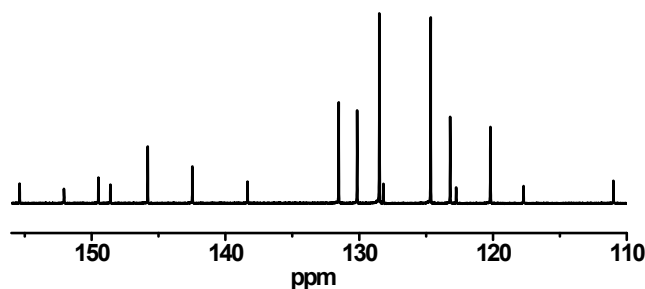
Figure S3 The ^{13}C NMR (CDCl$_3$, 600 MHz) graph of $_p$-TPA-PT-CN.

Section 2. Thermal Properties

The thermal stability of p-TPA-PT-CN were characterized by Differential scanning calorimetry (DSC) and Thermogravimetric analysis (TGA). As shown Figure S1a, the glass-transition temperature (T$_g$) of p-TPA-PT-CN is determined to be 87 °C, from the DSC traces during the second heating scans. As temperature elevation, the material appeared an exotherm at 153 °C caused by crystallization (T$_c$), followed by endotherm at 222 °C associated with melting (T$_m$) for p-TPA-PT-CN. Obviously, the enhanced inductive electron-withdrawing effect has a noticeable impact on the thermal properties of the materials. As we known, the thermal properties of the materials are determined by factors including interaction energies, electric

55555555554555

dipoles, molecular symmetry, et.al.
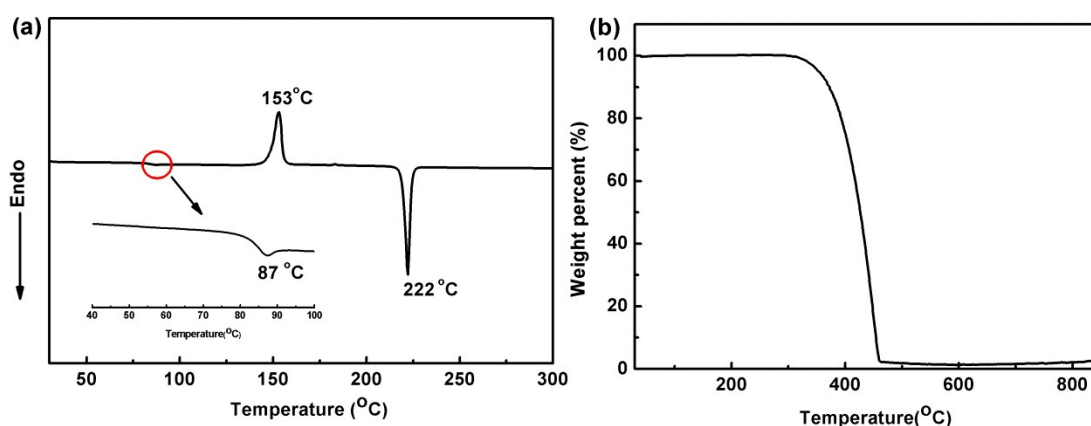
Figure S4. a) Second heating DSC traces of *p*-TPA-PT-CN in the temperature range of 40 °C and 300 °C (the insert figure is second heating DSC traces of the material in the temperature range of 40 °C and 100 °C); b) TGA thermographs of *p*-TPA-PT-CN.

It is possible that such improvement of thermal properties could be ascribed to increased more and/or stronger intermolecular interactions in the solid state arisen from the increased polarity of cyano-substituent. Benefitted from the same reason, the *p*-TPA-PT-CN exhibited high decomposition temperature (T_d, corresponding to 5% weight loss, 352 °C) evidently, the cyano-substituent significantly improve the thermal stability of the D-A materials, which is an important factor to get appreciable device performance.

Section 3. Photophysical Properties
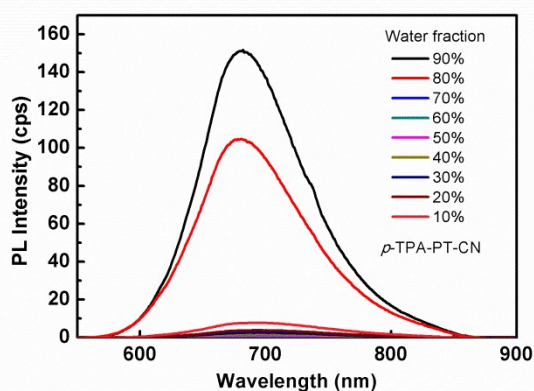
Figure S5. PL spectra of *p*-TPA-PT-CN (10^{-5} M) in THF/water mixtures with different water fractions.

we measured the PL spectra of *p*-TPA-PT-CN in THF/water mixtures with different water fractions (f_w, Figure S4). The solutions showed very weak emission when the f_w is less than 80

vol%. As the f_w increase to 80 vol%, the emission of the solution dramatically enhanced, indicating *p*-TPA-PT-CN has aggregation-induced-emission (AIE) characteristic.

Section 4. Solvatochromic effect and transient PL decay

The influence of solvent environment on the optical property of our compounds can be understood using the Lippert-Mataga equation[1-2], a model that describes the interactions between the solvent and the dipole moment of solute:

$$hc(v_a - v_f) = hc(v_a^0 - v_f^0) - \frac{2(\mu_e - \mu_g)^2}{a^3} f(\varepsilon, n)$$

where f is the orientational polarizability of solvents, μ_e is the excited-state dipole moment, μ_g is the ground-state dipole moment; a is the solvent cavity (Onsager) radius (6.69 Å), derived from the Avogadro number (N), molecular weight (M), and density (d=1.0 g/cm³); ε and n are the solvent dielectric and the solvent refractive index, respectively; $f(\varepsilon,n)$ and a can be calculated respectively as follows:

$$f(\varepsilon, n) = \frac{\varepsilon - 1}{2\varepsilon + 1} - \frac{n^2 - 1}{2n^2 + 1}, a = (3M/4N\pi d)^{1/3}$$
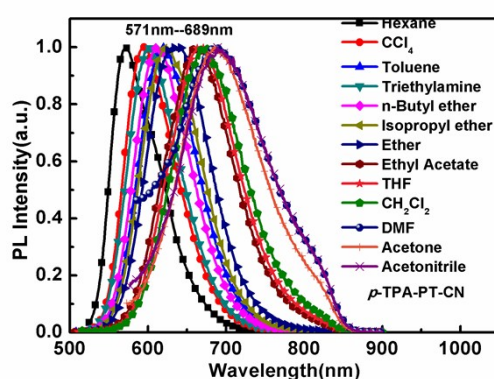
Figure S6. PL spectra of the *p*-TPA-PT-CN in different solvents with different polarity.

Table S1. Detailed photophysical data of *p*-TPA-PT-CN in different solvents.

solvent	Δf [nm]	λ_{ab}[a) [nm]	λ_{em}[b) [nm]	Stakes shift [cm^{-1}]	PLQY[c) [%]	$\mathcal{E}$[d) [10^4cm^{-1}M^{-1}]
Hexane	0.0012	505	571	2288	90.9	2.02
Tetrachloromethane	0.011	511	595	2762	90.3	1.39

Toluene	0.014	500	621	3896	81.2	1.91
Triethylamine	0.048	501	599	3265	16.0	1.17
n-Butyl ether	0.096	500	625	4000	80.1	2.09
Isopropyl ether	0.145	498	613	3767	70.1	1.97
Ether	0.167	494	639	4593	69.1	2.0
Ethyl Acetate	0.2	486	660	5424	15.7	1.89
tetrahydrofuran	0.21	491	668	5396	19.2	1.94
dichloromethane	0.217	495	667	5209	16.4	1.78
Dimethyl Formamide	0.276	485	687	6062	0.8	1.74
Acetone	0.284	481	685	6191	1.2	1.93
Acetonitrile	0.305	477	689	6450	0.8	1.92

[a)]Absorption maximum; [b)] Emission maximum; [c)] Fluorescence quantum yield estimated by using a integrating sphere; [d)] Molar extinction coefficient.
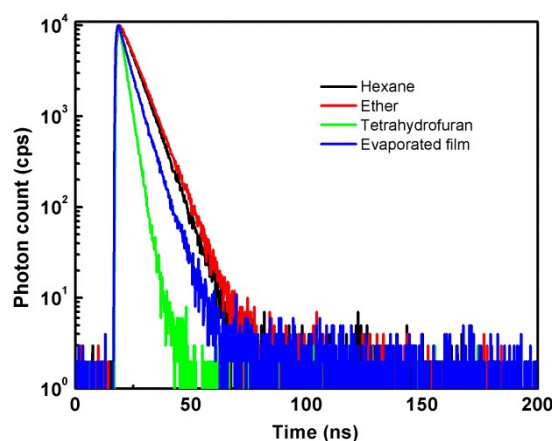
Figure S7. Transient PL decay profiles of the *p*-TPA-PT-CN in different solvents and films.

Table S2. Photophysical properties of *p*-TPA-PT-CN: quantum yields (ϕ_F), lifetime (τ_F), radiative (k_r) and non-radiative (k_{nr}) decay rates.

	Hexane[a]	Ether[a]	Tetrahydrofuran [a]	Evaporated film
ϕ_F[b]	0.91	0.69	0.29	0.28
τ_F [ns]	6.33	6.82	2.72	4.96
$k_r/10^7[s^{-1}]$[c]	14.36	10.13	7.06	5.56
$k_{nr}/10^7[s^{-1}]$[c]	1.44	4.53	29.71	14.60

[a)]concentration of 1.0×10^{-5} M; [b)]Absolue quantum yields determined with a calibrated integrating sphere system; [c)]k_r and k_{nr} were obtained by $k_r = \phi_F/\tau_F$; $\tau_F^{-1} = k_r + k_{nr}$.

Section5. Single crystal X-ray diffraction data and DFT calculations analysis

Single crystal of *p*-TPA-PT-CN were prepared by the slow diffusion of the CH_3OH (poor solvent) into the $CHCl_3$ (good solvent) solution at room temperature. The diffraction experiments

were carried out on a Xcalibur, Eos, Gemini diffractometer equipped with a CuKα or MoKα and Control Software using the RAPID AUTO at 293 (±2) °C. Empirical absorption corrections were applied multi-scan. The structures were solved with direct methods and refined with a full-matrix least-squares technique using the SHELXL-97 programs, respectively. The space groups were determined from the systematic absences and their correctness was confined by successful solution and refinement of structures. Anisotropic thermal parameters were refined for all the non-hydrogen atoms. The hydrogen atoms were added in idealized position and refined with isotropic displacement. Crystal date refinement conditions and experimental details are tabulated in table S3.

CCDC 1500956 contains the supplementary crystallographic data for this paper. These data are provided free of charge by The Cambridge Crystallographic Data Centre.
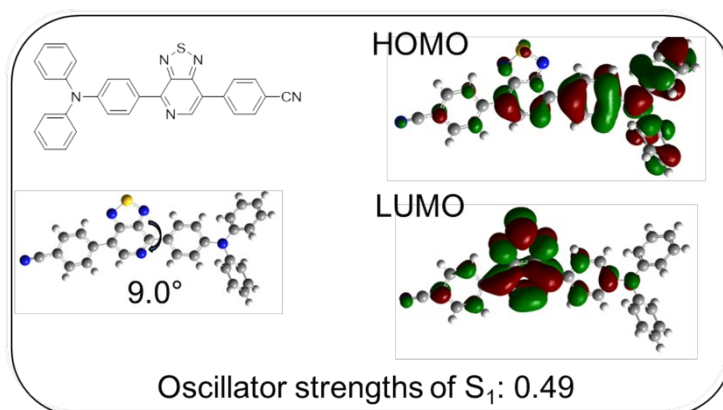
Figure S8. X-ray crystal structures and DFT calculations analysis of *p*-TPA-PT-CN.

Table S3. Crystallographic data and structure refinement for *p*-TPA-PT-CN.

Identification code	*p*-TPA-PT-CN
Empirical formula	$C_{30}H_{19}N_5S$
Formula weight	481.56
Temperature/K	293(2)
Crystal system	monoclinic
Space group	C2/c
a/Å	46.21(2)
b/Å	6.9886(10)
c/Å	24.593(13)
α/°	90.00
β/°	144.02(11)
γ/°	90.00
Volume/Å^3	4666(3)

Z	8
ρ_{calc}g/cm^3	1.371
μ/mm^{-1}	1.465
F(000)	2000.0
Radiation	CuK$^\alpha$(λ=1.54184)
2$^\Theta$range for datacollection/°	6.52 to 134.5
Reflections collected	7825
Data/restraints/parameters	4194/0/326
Goodness-of-fit on F^2	0.994
Final R indexes [I>=2σ (I)]	R_1 = 0.0686, wR_2 = 0.1527
Final R indexes [all data]	R_1 = 0.1467, wR_2 = 0.2366
Largest diff. peak/hole / e Å^{-3}	0.36/-0.41

Section6. Electroluminescence Performances
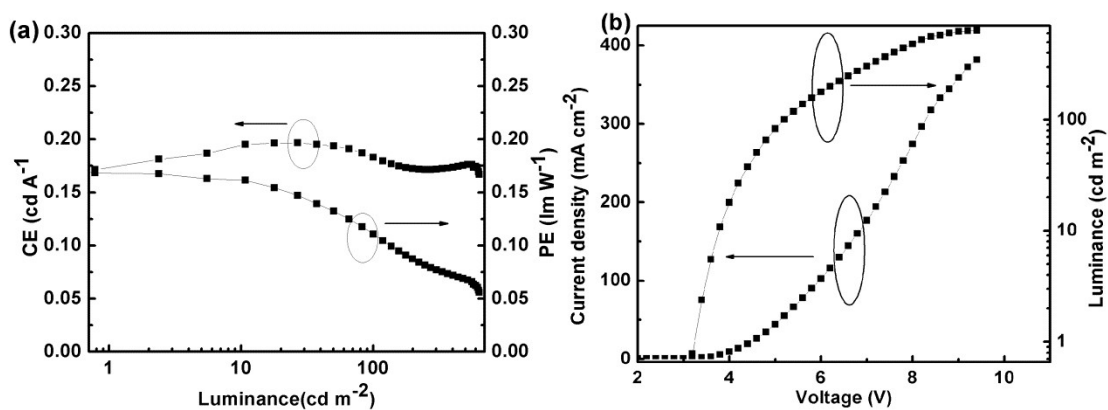
Figure S9. Curves of luminous efficiency versus current density (a) and the J–V–L characteristics (b) of NIR device based on the material.

TableS4. The luminous efficiency of organic small-molecule NIR emitters.

Compound	Structure	λ_{em} (nm) / EQE (%)
p-TPA-PT-CN(this work)		700/1.47
NZ2TPA (Ref 28)		696/3.9
TPA-DCPP (Ref 21)		708/2.1
TPATCN (Ref 27)		675/2.58
PTZ-BZP (Ref 20)		700/1.54
NZ2AC (Ref 29)		663/2.8
TPA-QCN (Ref 30)		728/3.9

Reference:

[1] V. E. Z. Lippert, *Electrochemistry* **1957**, *61*, 962.

[2] N. Mataga, Y. Kaifu, M. Koizumi, *Bull. Chem. Soc. Jpn.* **1956**, *29*, 465.

11111111111111111111114111111